work on elucidating the mechanism of this remarkable transformation is in progress.

In contrast to **2**, the $VO(EHPG)^-$ structure presented herein may not represent the vanadyl analogue of the reactive V^{5+} species. The existence of this compound requires an acidic medium to protonate a phenolate moiety. In DMF, we would expect that the phenol is directly associated with the V^{5+} ion and that the uncoordinated arm is the carboxylate moiety, which is not subject to the first oxidative decarboxylation. Further details of this chemical transformation are reported elsewhere.[10]

Summary

We report the structures of a series of vanadyl complexes that are associated with a novel stepwise oxidative decarboxylation of VO(EHPG) to VO(SALEN). Isolation of the $VO(EHGS)^-$ complex, a structural analogue of the reactive VO(EHGS) intermediate, demonstrates that the carboxylate moiety is directly coordinated to metal, and this in turn supports an intramolecular mechanism for the decarboxylation pathway. That VO(SALEN) is the final product of the reaction scheme is proven by crystal structure analysis.

Acknowledgment. This research was supported by NIH Grant HL 24775 (now Grant AM-32999).

Registry No. 1, 99016-50-9; **2**, 89890-30-2; **3**, 36913-44-7.

Supplementary Material Available: Table V [anisotropic thermal parameters for $[NH_4][VO(EHPG)]\cdot H_2O\cdot C_2H_5OH$], Table VI [anisotropic thermal parameters for $Na[VO(EHGS)]\cdot 1.5H_2O\cdot CH_3OH$], Table VII [anisotropic thermal parameters for VO(SALEN)], Table VIII [hydrogen atom parameters for $[NH_4][VO(EHPG)]\cdot H_2O\cdot C_2H_5OH$], Table IX [hydrogen atom parameters for $Na[VO(EHGS)]\cdot 1.5H_2O\cdot CH_3OH$], Table X [hydrogen atom parameters for VO(SALEN)], Table XI [structure factor amplitudes for $[NH_4][VO(EHPG)]\cdot H_2O\cdot C_2H_5OH$], Table XII [structure factor amplitudes for $Na[VO(EHGS)]\cdot 1.5H_2O\cdot CH_3CH_3OH$], Table XIII [structure factor amplitudes for VO(SALEN)], Table XVII [selected intermolecular distances (Å) for $[NH_4][VO(EHPG)]\cdot H_2O\cdot C_2H_5OH$], Table XVIII [selected mean planes in **1**-**3**], and Table XIX [selected intermolecular distances (Å) for $Na[VO(EHGS)]\cdot 1.5H_2O\cdot CH_3OH$] (63 pages). Ordering information is given on any current masthead page.

Contribution from the School of Chemical Sciences, University of Illinois, Urbana, Illinois 61801

Dynamics of Spin-State Interconversion and Cooperativity for Ferric Spin-Crossover Complexes in the Solid State. 6.[1] Magnetic and Spectroscopic Characterizations of $[Fe(3\text{-}OEt\text{-}SalAPA)_2]X$ ($X = ClO_4^-$, BPh_4^-)

Mark D. Timken, A. M. Abdel-Mawgoud, and David N. Hendrickson*

Received May 21, 1985

The spin-crossover transformation is examined for two ferric complexes of the composition $[Fe(3\text{-}OEt\text{-}SalAPA)_2]X$, where X is either ClO_4^- or BPh_4^- and 3-OEt-SalAPA is the monoanionic Schiff base derived from 3-ethoxysalicylaldehyde and *N*-(3-aminopropyl)aziridine. Variable-temperature magnetic susceptibility, EPR, and Mössbauer data are analyzed for these two complexes. Both are seen to undergo spin-crossover transformations that are more gradual than that observed for the benzene solvate of the $X = ClO_4^-$ compound, which was studied in the previous paper in this series. EPR spectra of the two complexes in this study show that both have d_{xy} low-spin ground states. More importantly, it is found that the two complexes interconvert slower than the EPR time scale but faster than the ^{57}Fe Mössbauer time scale. This shows that neither desolvating the $X = ClO_4^-$ benzene solvate nor replacing the ClO_4^- anion by the BPh_4^- counterion measurably reduces the rate of spin flipping of the $[Fe(3\text{-}OEt\text{-}SalAPA)_2]^+$ cation.

Introduction

The study of solid-state spin-crossover transformations affords a means for examining the coupling of an intramolecular process, the high-spin $\rightleftharpoons$ low-spin interconversion, to the intermolecular interactions inherent to the solid state. In the ferric case, the spin-crossover event involves an intramolecular transfer of the two electrons between the t_{2g}-type and e_g-type d orbitals. Due to the antibonding character of the e_g orbitals, significant metal-ligand bond length changes accompany the spin-state interconversion process. The solid must be able to accommodate these coordination sphere contractions and expansions if molecules of both spin states are to reside within the *same* lattice. Although it has been shown[2] that thermally discontinuous spin-crossover transformations are accompanied by discontinuous lattice changes, it has also been demonstrated[1,3,4] that dramatic lattice rearrangements do not usually accompany thermally gradual transformations. Instead, the lattice parameters show gradual temperature-dependent changes. Recent efforts in spin-crossover research have centered to a large extent on determining the factors that influence the *bulk* properties of the solid-state transformation. It is important, as well, to gain some understanding of the means by which intermolecular interactions inhibit or enhance the *rates* of intramolecular spin-state interconversions.

These solid-state rates have typically been estimated relative to the time scales associated with various spectroscopic techniques (e.g., for Mössbauer $\tau \approx 10^{-7}$ s and for EPR $\tau \approx 10^{-10}$ s). Until recently, only the ferric dithiocarbamates,[5] monothiocarbamates,[6] and diselenocarbamates[7] have been shown to interconvert spin states rapidly on the Mössbauer time scale. Within the past few years, however, a number of ferric complexes with N_4O_2 ligand atom donor sets have also been shown[1,8-13] to interconvert rapidly

(1) Part 5: Timken, M. D.; Strouse, C. E.; Soltis, S. M.; Daverio, S.; Hendrickson, D. N.; Abdel-Mawgoud, A. M.; Wilson, S. R. *J. Am. Chem. Soc.*, in press.
(2) König, E.; Ritter, G.; Irler, W.; Goodwin, H. A. *J. Am. Chem. Soc.* **1980**, *102*, 4681.
(3) König, E.; Ritter, G.; Kulsbreshtha, S. K.; Nelson, S. M. *J. Am. Chem. Soc.* **1983**, *105*, 1924.
(4) (a) Albertsson, J.; Oskarsson, A. *Acta Crystallogr. Sect. B: Struct. Crystallogr. Cryst. Chem.* **1977**, *B33*, 1871. (b) Albertsson, J.; Oskarsson, A.; Stahl, K.; Svenson, C.; Ymen, I. *Acta Crystallogr. Sect. B: Struct. Crystallogr. Cryst. Chem.* **1981**, *B37*, 50.
(5) Merrithew, P. B.; Rasmussen, P. G. *Inorg. Chem.* **1972**, *11*, 325.
(6) Kunze, K. R.; Perry, D. L.; Wilson, L. J. *Inorg. Chem.* **1977**, *16*, 594.
(7) DeFilipo, D.; Depalano, P.; Diaz, A.; Steffe, S.; Trogu, E. F. *J. Chem. Soc., Dalton Trans.* **1977**, 1566.
(8) Maeda, Y.; Tsutsumi, N.; Takashima, Y. *Chem. Phys. Lett.* **1982**, *88*, 248.
(9) Maeda, Y.; Ohshio, H.; Takashima, Y. *Chem. Lett.* **1982**, 943.
(10) Ohshio, H.; Maeda, Y.; Takashima, Y. *Inorg. Chem.* **1983**, *22*, 2684.
(11) Maeda, Y.; Tsutsumi, N.; Takashima, Y. *Inorg. Chem.* **1984**, *23*, 2440.
(12) Federer, W. D.; Hendrickson, D. N. *Inorg. Chem.* **1984**, *23*, 3861.

0020-1669/86/1325-0160$01.50/0

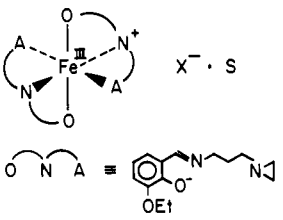

I: X^- = ClO_4^-, no solvate
II: X^- = ClO_4^-, S = benzene
III: X^- = BPh_4^-, no solvate

Figure 1. Structure of the $[Fe(3\text{-}OEt\text{-}SalAPA)_2]^+$ cation and listing of the compounds studied in this paper.

relative to the Mössbauer time scale. Relevant to the effect of intermolecular interactions on these rates, Maeda et al.[11] have recently noted that relatively subtle structural perturbations can dramatically alter the spin-state interconversion rates in the solid state. In particular, these workers found a particular ferric N_4O_2 solid that could be made to interconvert rapidly or slowly relative to the Mössbauer time scale simply by changing the counterion. The microscopic origin of such a subtle effect is not known, especially in view of the lack of crystallographic information on many of these spin-crossover systems. Recently, in collaboration with Strouse and co-workers, we reported[1] the spectroscopic, magnetic, and structural characterization of $[Fe(3\text{-}OEt\text{-}SalAPA)_2]ClO_4 \cdot C_6H_6$, where 3-OEt-SalAPA is the monoanionic form of the Schiff-base condensate of 3-ethoxysalicylaldehyde and *N*-(3-aminopropyl)aziridine. This solid, which exhibits rapid spin-state interconversion on the Mössbauer time scale and slow interconversion on the EPR time scale, was examined with single-crystal X-ray diffraction methods at temperatures ranging from 300 to 20 K. It was concluded that a rapid solid-state reorganization (local or extended) may be leading to more facile spin-state interconversions.

In light of Maeda's report[11] of the sensitivity of the spin-state interconversion rates to counterion changes, we were motivated to investigate the properties of the molecular cation $[Fe(3\text{-}OEt\text{-}SalAPA)_2]^+$ in several lattice environments. In this paper, the results of spectroscopic and magnetic examinations of the two new spin-crossover solids $[Fe(3\text{-}OEt\text{-}SalAPA)_2]BPh_4$ and $[Fe(3\text{-}OEt\text{-}SalAPA)_2]ClO_4$ are reported.

Experimental Section

Compound Preparation. Reagents were obtained as described previously.[12] The ^{57}Fe powder (95% enriched) was obtained from New England Nuclear. Elemental analyses were performed in the Microanalytical Laboratory of the School of Chemical Sciences, University of Illinois.

$[Fe(3\text{-}OEt\text{-}SalAPA)_2]ClO_4$. This sample was prepared with 95%-enriched ^{57}Fe powder as described previously.[1] Anal. Calcd for $FeC_{28}N_4O_8H_{38}Cl$: C, 51.65; H, 5.88; N, 8.60. Found: C, 50.32; H, 5.62; N, 8.35.

$[Fe(3\text{-}OEt\text{-}SalAPA)_2]BPh_4$. This material was obtained by metathesis of the ClO_4^- salt in MeOH with $NaBPh_4$ (4-fold molar excess). The dark powder thus obtained was recrystallized from boiling MeOH to give deep purple microcrystals, which were isolated by filtration and air-dried. Anal. Calcd for $FeC_{52}H_{58}O_4N_4B$: C, 71.81; H, 6.72; N, 6.44. Found: C, 71.83; H, 6.60; N, 6.42.

Methods. The magnetic, spectroscopic, and X-ray diffraction methods that were used are described elsewhere.[1]

Results and Discussion

Molecular Structure. Single-crystal X-ray diffraction studies[1] of $[Fe(3\text{-}OEt\text{-}SalAPA)_2ClO_4 \cdot C_6H_6$ have shown that the molecular cation adopts the centrosymmetric geometry pictured in Figure 1. The unsolvated ClO_4^- and BPh_4^- samples, hereafter referred to as I and III, respectively, undoubtedly retain the same molecular geometry as found for II. Room-temperature powder X-ray diffraction patterns indicate that the three solids are not isostructural, however. Although a complete description of the properties of II has been published previously, occasionally data will be included for this compound for comparative purposes.

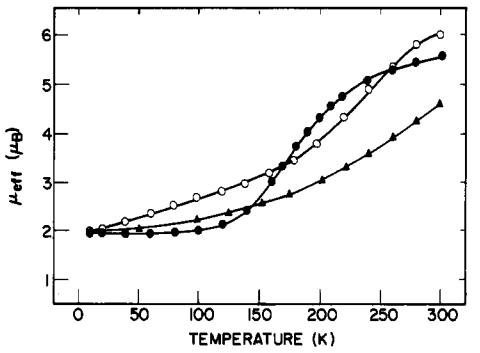

Figure 2. Magnetic moment vs. temperature curves for I (▲), II (●), and III (○). Solid lines are drawn for clarity only and do not represent data fittings or simulations.

Magnetic Susceptibility. As illustrated in Figure 2 (and tabulated elsewhere[14]), all three solids undergo gradual spin-crossover transformations. For II and III the transformations are nearly complete, whereas I shows appreciable low-spin population (ca. 46%) at room temperature. It has been well established that counterions[15,16] and solvate[17] molecules change the thermodynamics of the *bulk* solid-state spin-crossover transformation. These changes are often unpredictable and seemingly result from the effect of subtle lattice forces in stabilizing one spin state relative to the other. Nevertheless, in the series I–III, it is tempting to suggest that the high-spin molecules in II and III are favored due to the lattice expansions resulting from the benzene solvate and the large BPh_4^- counterion.

It is evident in Figure 2 that the three solids exhibit three distinctly different shapes of the μ_{eff} vs. temperature curves. If temperature-independent values are assumed for the low-spin and high-spin effective magnetic moments, the high- and low-spin population fractions can be estimated. Consequently, equilibrium constants (K_{eq} = [HS]/[LS]) can be calculated as a function of temperature, and it is often possible to estimate the enthalpies and entropies for spin-crossover "reactions" from plots of ln K_{eq} vs. reciprocal temperature. As noted previously,[1] II yields a very linear ln K_{eq} vs. $1/T$ curve for over 77% of the spin-crossover transformation. The distinctly different μ_{eff} vs. T curves for I and III yield nonlinear ln K_{eq} vs. $1/T$ curves. Nonlinearities for I and III cannot necessarily be interpreted as evidence for cooperativity in the spin-crossover transformation; solid-state transformations can exhibit nonlinear ln K_{eq} vs. $1/T$ behavior for a variety of circumstances.[18]

Electron Paramagnetic Resonance. In Figures 3 and 4 are illustrated the X-band EPR spectra at a number of temperatures for I and III, respectively. As expected, the gradual nature of the spin-crossover transformation in each case is apparent. The low-spin rhombic **g**-tensor resonances near $g = 2$ increase in intensity at the expense of the high-spin $g \simeq 4$ resonance as the temperature is lowered. That III undergoes a more complete transformation than does I is also evident.

It is important to note that the observation of *distinct* high- and low-spin resonances implies that the spin-state interconversion rates in the region of 77–300 K are slower than $\sim 10^{10}$ s^{-1} (the EPR spectra time scale). Similar observations were reported for II.[1]

An expanded view of the low-spin **g** tensors for I–III and for I (10^{-3} M in EtOH) is illustrated in Figure 5. All of the samples

(13) Federer, W. D.; Hendrickson, D. N. *Inorg. Chem.* **1984**, *23*, 3870.

(14) Supplementary material.
(15) Gütlich, P. *Struct. Bonding (Berlin)* **1981**, *44*, 83.
(16) Haddad, M. S.; Lynch, M. W.; Federer, W. D.; Hendrickson, D. N. *Inorg. Chem.* **1981**, *20*, 123.
(17) Malliaris, A.; Papaefthimiou, V. *Inorg. Chem.* **1982**, *21*, 770.
(18) Linear ln K_{eq} vs. $1/T$ relationships do not result if the enthalpy difference between the high- and low-spin states is temperature-dependent or if the heat capacity difference is temperature-dependent. For a brief discussion, see: Rock, P. A. "Chemical Thermodynamics"; Macmillan: London, 1969; pp 188–9.

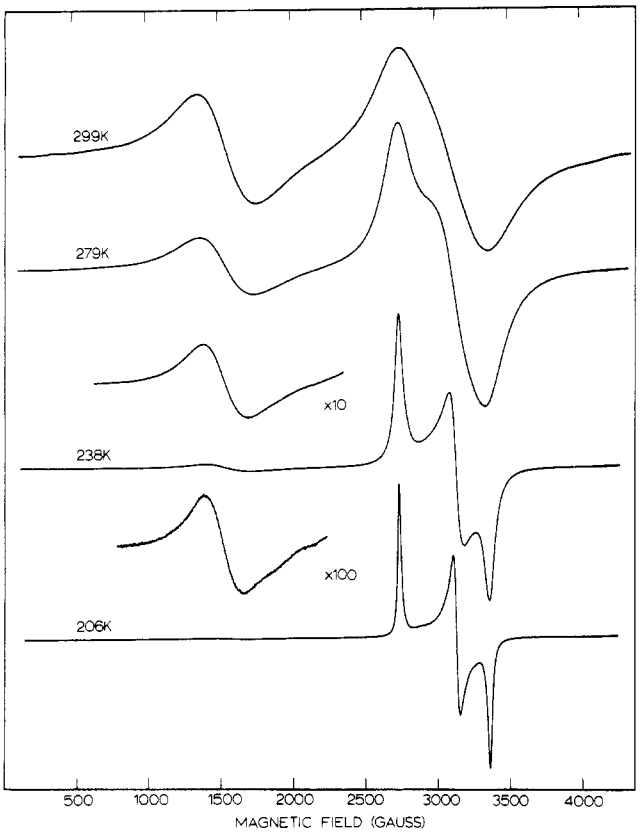

Figure 3. X-Band EPR spectra of I at representative temperatures.

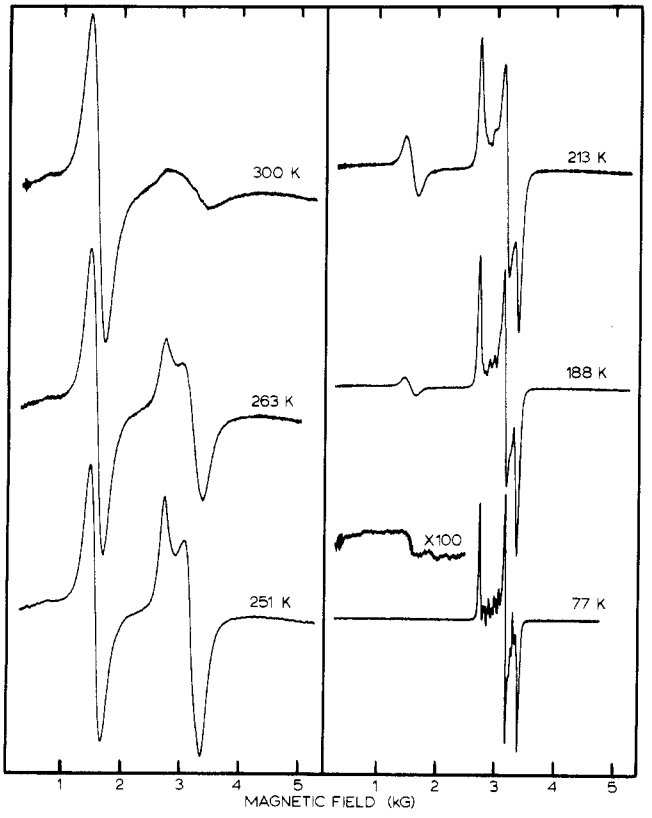

Figure 4. X-Band EPR spectra of III at representative temperatures.

exhibit rhombic g-tensor resonances, consistent with the suggestion that the molecular geometries for the samples are quite similar. The low-spin ferric g values, listed in Table I, were analyzed by the method of Bohan.[19] Specifically, the g values were used to

(19) Bohan, T. L. *J. Magn. Reson.* **1977**, *26*, 109.

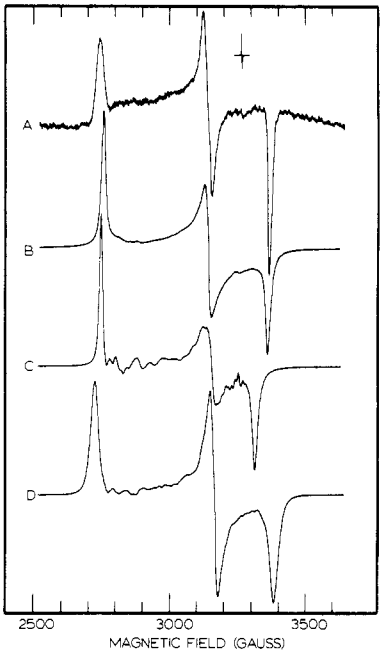

Figure 5. X-Band EPR spectra at 77 K for I (B), II (C), III (D), and I 10^{-3} M in EtOH (A).

Table I. Experimental and Calculated[a] EPR Parameters

	I	II	III	I (10^{-3} M in EtOH)
g_x	−2.371	−2.379	−2.400	−2.382
g_y	2.079	2.077	2.065	2.083
g_z	−1.946	−1.974	−1.933	−1.943
k	0.959	1.406	0.910	0.966
A	−0.0432	−0.0258	−0.0463	−0.0447
B	−0.9990	−0.9996	−0.9988	−0.9989
C	0.0146	0.0096	0.0168	0.0150
E_1/λ	−12.67	−21.60	−12.06	−12.22
E_2/λ	−0.42	−1.62	−0.85	−0.36
E_3/λ	12.08	22.22	11.91	11.57

[a] Parameter definitions and methods of calculation are described in text.

determine the nature of the ground-state Kramers doublet. With the use of the Hamiltonian

$$H = -\lambda \mathbf{l}\cdot\mathbf{s} + (\mu/9)(3\mathbf{l}_z^2 - \mathbf{l}(\mathbf{l}+1)) + (\mathbf{R}/12)(\mathbf{L}_+^2 + \mathbf{L}_-^2)$$

acting upon the appropriate one-electron orbitals for the t_{2g}^5 configuration, three secular equations result for the Kramers doublet. In the Hamiltonian, λ is the spin–orbit coupling constant, μ is the axial ligand field distortion parameter, and **R** gauges the rhombic distortion. By using the Zeeman Hamiltonian in conjunction with the wave functions obtained from the aforementioned secular equations, we obtain the expressions

$$g_z = -2[A^2 - B^2 + C^2 + k(A^2 - C^2)]$$

$$g_x = 2[2AC - B^2 + kB(2^{1/2})(C - A)]$$

$$g_y = -2[2AC + B^2 + kB(2^{1/2})(C + A)]$$

where k is the orbital reduction factor and A, B, and C characterize the ground-state Kramers doublet. That is

$$\psi = A|+1^+\rangle + B(1/2)^{1/2}[|2^-\rangle - |-2^-\rangle] + C|-1^+\rangle$$

$$\psi' = A|-1^-\rangle - B(1/2)^{1/2}[|2^+\rangle - |-2^+\rangle] + C|1^-\rangle$$

The experimental g values were computer least-squares fit to the g-value expressions and the normalization condition ($A^2 + B^2 + C^2 = 1.0$) to give A, B, C, and k values listed in Table I. In addition, the energies of the three Kramers doublets of $^2T_{2g}$ origin (E_1/λ, E_2/λ, and E_3/λ) were obtained by solving the secular equations; these values are also listed in Table I.

Table II. Mössbauer Parameters for $[Fe(3\text{-}OEt\text{-}SalAPA)_2]ClO_4$ (I) (Two-Line Lorentzian Fits)[a]

T, K	CS, mm/s	QS, mm/s	Γ_-, mm/s[b]	Γ_+, mm/s[c]	ln (area)[d]	χ^2[e]
300[f]	0.264 (1)	1.263 (2)	0.337 (2)	0.362 (2)	1.380	0.79
285[f]	0.267 (1)	1.379 (1)	0.354 (1)	0.352 (2)	1.508	0.82
271[f]	0.267 (1)	1.547 (1)	0.367 (2)	0.335 (2)	1.646	1.65
256[f]	0.261 (1)	1.752 (2)	0.365 (2)	0.314 (2)	1.777	6.02
241[f]	0.257 (1)	1.954 (2)	0.347 (3)	0.288 (2)	1.884	14.30
227[f]	0.251 (1)	2.117 (2)	0.322 (3)	0.260 (2)	1.976	12.38
212[f]	0.248 (1)	2.229 (2)	0.297 (2)	0.233 (2)	2.047	18.95
192[f]	0.251 (1)	2.325 (2)	0.280 (2)	0.218 (2)	2.138	9.09
160[g]	0.257 (1)	2.445 (1)	0.244 (1)	0.183 (1)	1.666	1.48
130[g]	0.266 (1)	2.470 (1)	0.245 (1)	0.186 (1)	1.804	1.65
110[g]	0.272 (1)	2.477 (1)	0.243 (1)	0.185 (1)	1.881	1.84

[a] Parameters obtained by assuming unequal areas for the two component peaks of the quadrupole doublet. [b] Half-width at half-height of the negative-velocity component. [c] Half-width at half-height for the positive-velocity component. [d] Natural logarithm of background-normalized area of total fitted spectrum. [e] χ^2 value indicating quality of data and of fit to seven adjustable parameters. [f] 12-mg sample. [g] 3-mg sample.

Table III. Mössbauer Parameters for $[Fe(3\text{-}OEt\text{-}SalAPA)_2]BPh_4$ (III) (Two-Line Lorentzian Fits)[a,g]

T, K	IS, mm/s	QS, mm/s	Γ_-, mm/s[b]	Γ_+, mm/s[c]	ln (area)[d]	χ^2[e]
296	0.337 (3)	1.311 (6)	0.532 (5)	0.840 (8)	1.476	1.31
282	0.341 (3)	1.285 (6)	0.564 (5)	0.860 (8)	1.587	1.75
257	0.288 (3)	1.323 (5)	0.638 (5)	0.844 (7)	1.809	2.63
238	0.272 (2)	1.545 (4)	0.705 (4)	0.756 (5)	1.960	1.96
218	0.253 (2)	1.884 (4)	0.733 (4)	0.632 (3)	2.094	2.14
199	0.245 (2)	2.219 (4)	0.717 (4)	0.508 (3)	2.211	2.41
169	0.242 (2)	2.502 (4)	0.619 (5)	0.374 (3)	2.337	5.51
139	0.254 (2)	2.593 (4)	0.543 (5)	0.318 (3)	2.392	8.07
139[f]	0.256 (1)	2.593 (2)	0.619 (4)	0.305 (1)	2.451	1.61
121	0.260 (2)	2.603 (5)	0.516 (6)	0.308 (3)	2.514	13.76
121[f]	0.262 (1)	2.602 (2)	0.600 (3)	0.292 (1)	2.573	1.92

[a] Parameters obtained by assuming equal areas for the two component peaks of the quadrupole doublet. [b] Half-width at half-height of the negative-velocity component. [c] Half-width at half-height for the positive-velocity component. [d] Natural logarithm of background-normalized area of total fitted spectrum. [e] χ^2 value indicating quality of data and of fit to six adjustable parameters. [f] Peaks fit to unequal quadrupole components (seven adjustable parameters). [g] 7-mg sample.

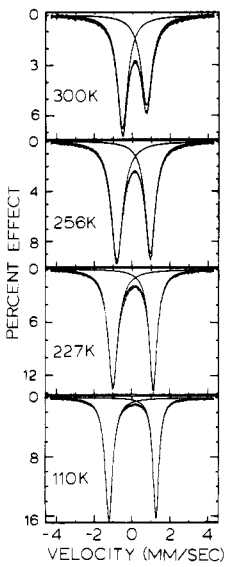

Figure 6. Representative ^{57}Fe Mössbauer spectra of I. Solid lines represent fittings to Lorentzian line shapes.

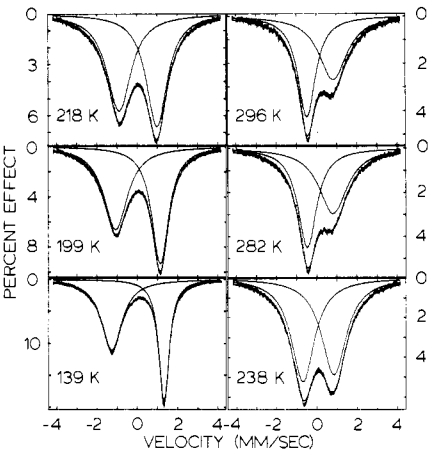

Figure 7. Representative ^{57}Fe Mössbauer spectra of III. Solid lines represent fittings to Lorentzian line shapes.

Several important conclusions are to be drawn from the analyses of these g values. First we note from Table I that in each case the unpaired electron in the ground Kramers doublet is in essentially a d_{xy} orbital ($B = 1.0$). This observation has implications regarding the low-spin Mössbauer data to be discussed later. Furthermore, if we take the spin–orbit coupling constant to be 460 cm^{-1}, then the energy separation of the ground and first excited Kramers doublets is $\sim$5000 cm^{-1}, a value much larger than thermal energies. Consequently, the low-spin magnetic moment and Mössbauer quadrupole splitting are expected to be temperature-independent, and the temperature dependencies of these quantities can be attributed solely to spin-crossover origins. Finally, due to the low-field shift of g_z, II analyzes to give a nonsensible orbital reduction factor greater than 1.0. It is quite likely that very weak intermolecular magnetic exchange interactions between crystallographically independent ferric centers are responsible for this anomaly.

Mössbauer Spectroscopy. As noted in the Introduction, the use of Mössbauer spectroscopy has been instrumental in determining the intramolecular spin-state interconversion rates in spin-crossover solids. Due to the poor recoilless fractions of the samples studied here, all of the data were obtained with the use of 95%-enriched ^{57}Fe samples. Figures 6 and 7 illustrate representative Mössbauer spectra for I and III, respectively. As was the case for II, both I and III exhibit at each temperature a single quadrupole-split doublet with a temperature-dependent splitting, from which we can infer that the spin-state interconversion rates are more rapid than $\sim 10^7$ s^{-1}. The spectra were computer fit to Lorentzian line shapes, and the relevant parameters are listed in Tables II and III.

Even though I–III all exhibit rapid spin-state interconversion on the Mössbauer time scale, there are noticeable differences

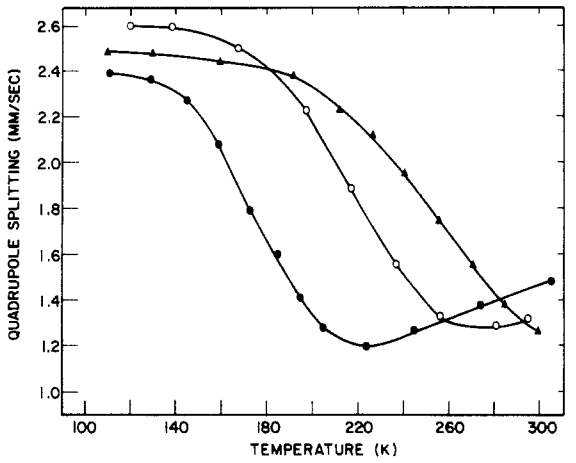

Figure 8. Quadrupole splittings vs. temperature curves for I (▲), II (●), and III (○).

between the appearances of their respective spectra. For example, the line widths are much broader for III than for I. Additionally, III exhibits marked line width asymmetries, whereas the asymmetries for I, although present, are much less visually apparent. These differences can be attributed primarily to differences in the electron spin relaxation times for I and III. If the spin–spin and/or spin–lattice relaxation times are not rapid relative to the ^{57}Fe nuclear Larmor precession frequency, then an appreciable internal magnetic field can broaden the Mössbauer absorptions of any paramagnetic sample. As pointed out by Blume,[20] intermediate paramagnetic relaxation broadens the $|I = {}^1/_2, M_I = \pm{}^1/_2\rangle \rightarrow |{}^3/_2, \pm{}^3/_2\rangle$ quadrupolar component more than it broadens the $|{}^1/_2, \pm{}^1/_2\rangle \rightarrow |{}^3/_2, \pm{}^1/_2\rangle$ component. At low temperatures where I and III are largely low spin, the negative-velocity quadrupolar component is broader than the positive-velocity component for both samples. From this it can be inferred that the principal-axis component of the electric field gradient tensor, V_{zz}, is negative, a result consistent with the d_{xy} ground state indicated by EPR g-tensor analyses. The generally broader line widths for III relative to I indicate that the electron spin relaxation times are consistently longer for III than for I. It is very likely that this is a reflection of the size of the counterion. Spin–spin relaxation mechanisms, dipolar in nature, are expected to be attenuated in III, where the large BPh_4^- anion effectively isolates the paramagnetic centers. That spin–spin mechanisms play a major role in the paramagnetic relaxation rates is suggested by the successive increase in line widths across the series I–III.

It is readily apparent from Figure 7 that the line width asymmetry at room temperature is opposite to that observed at 139 K. Similar observations were made for II[1] and, to a lesser extent, for I. It is clear that V_{zz} is positive for the essentially high-spin species. It is not unreasonable that the signs of V_{zz} are opposite for the low- and high-spin electronic states of the same molecule. The origins of the electric field gradient (EFG) tensors in the two cases are completely different. For the low-spin electronic state the EFG tensor results primarily from the asymmetric contribution of valence electrons. In the high-spin case, the valence EFG contribution is negligible and the EFG originates largely in the lattice charges that surround the ^{57}Fe nucleus.

One result of the opposite signs of V_{zz} for the low- and high-spin electronic states is the temperature dependence of the quadrupole splitting illustrated in Figure 8. As pointed out by Maeda[21] and discussed in some detail in the preceding paper[1] in this series, a minimum in the quadrupole splitting is *expected* at some population ratio of high spin to low spin. Both II and III exhibit such a minimum, although at different temperatures and different population ratios of high to low spin. As was pointed out previously,[1] the population ratio at which this minimum occurs is a sensitive function of the relative magnitudes of the V_{zz} values, the relative orientations of the EFG tensors of the high- and low-spin species, and the extent of deviation of each tensor from nonaxial symmetry. Considering all of these variables and the fact that the lattice contributions to the EFG tensor will be highly dependent upon the solid-state structure, it is not at all surprising that II and III show quadrupole splitting minima at different high-spin to low-spin population ratios. For I, it is likely that the quadrupole splitting minimum will occur at temperatures greater than 300 K.

Conclusions

From these results it is clear that although lattice features modulate the bulk properties of the spin-crossover transformation for [Fe(3-OEt-SalAPA)$_2$]X, the spin-state interconversion rates are not *measurably* affected. In all three lattices (X = ClO_4^-, benzene-solvated X = ClO_4^-, X = BPh_4^-) the spin-state interconversion rates are rapid relative to the Mössbauer spectroscopic time scale ($>10^7$ s^{-1}) and slow relative to the EPR time scale ($<10^{10}$ s^{-1}). Following our previous suggestion,[1] it is possible that rapid solid-state reorganizations are responsible for the rapid spin-state interconversions in all three materials, although such a suggestion is only tentative considering the lack of any structural characterization of samples I and III. It is also possible that *inter*molecular steric interactions in all three of the solids are too weak to raise effectively the reorganizational energy barriers that accompany the intramolecular spin-state interconversion process. Since strong intermolecular interactions, e.g., hydrogen bonding, are probably not present in any of these solids, it is perhaps not too surprising that all three exhibit rapid spin-state interconversions.

Acknowledgment. We are grateful for support from NIH Grant HL13652.

Registry No. I, 99572-41-5; III, 99664-00-3.

Supplementary Material Available: Tables of magnetic susceptibility data (2 pages). Ordering information is given on any current masthead page.

(20) Blume, M. *Phys. Rev. Lett.* **1965**, *14*, 96.

(21) Maeda, Y.; Takashima, Y. *Mem. Fac. Sci., Kyushu Univ., Ser. C* **1983**, *14*, 107.